

A sample of 6C radio sources designed to find objects at redshift > 4 : I — the radio data

Katherine M. Blundell¹, Steve Rawlings¹, Stephen A. Eales²
 Gregory B. Taylor³ & Alistair D. Bradley^{1,4}

¹*Astrophysics, Department of Physics, Keble Road, Oxford, OX1 3RH, U.K.*

²*Department of Physics and Astronomy, University of Cardiff, Wales, U.K.*

³*National Radio Astronomy Observatory, Socorro, NM 87801, U.S.A.*

⁴*Present address: Superconductivity Research Group, University of Birmingham, B15 2TT, U.K.*

28 April 2018

ABSTRACT

We describe the selection of a sample of 34 radio sources from the 6C survey (Hales, Baldwin & Warner 1993) from a region of sky covering 0.133 sr. The selection criteria for this sample, hereafter called 6C*, were chosen to optimise the chances of finding radio galaxies at redshift $z > 4$. Optical follow-up observations have already led to the discovery of the most distant known radio galaxy at $z = 4.41$ (Rawlings et al. 1996). We present VLA radio maps and derive radio spectra for all the 6C* objects.

Key words: radio continuum: galaxies – galaxies: active

1 INTRODUCTION

The primary goal of this study was to find radio galaxies with redshift > 4 . Such systems probe the Universe about 10^9 years after the Big Bang (we assume throughout that $H_0 = 50 \text{ km s}^{-1} \text{ Mpc}^{-1}$, $q_0 = 0.5$ and that the cosmological constant is zero) and may inform on the early evolutionary history of elliptical galaxies (e.g., Eales & Rawlings 1996). This study can also be viewed as part of a larger programme designed to measure the cosmic evolution of the co-moving density ρ of radio-loud objects (e.g., Dunlop & Peacock 1990).

The considerable difficulties involved in finding $z > 4$ radio galaxies are illustrated by Fig. 1. Such objects are absent from the brightest radio source samples (e.g., the revised 3CR sample: Laing, Riley & Longair 1983) because of an upper limit to the low-frequency (151 MHz) radio luminosity L_{151} of radio sources of $\log_{10} L_{151} < 28.8$ (where we measure L_{151} in units of $\text{W Hz}^{-1} \text{ sr}^{-1}$). Radio sources at $z > 4$ may be present in fainter low-frequency selected samples (see Fig. 1) but only amongst a much larger number of less distant radio sources; the *fraction* of radio-luminous $z > 4$ radio galaxies in a flux-limited sample declines as the flux limit is decreased even if there is

no high-redshift cutoff in ρ (Fig. 1). At most only about 1 per cent of a complete sample selected at a 151-MHz flux density $S_{151} \approx 1 \text{ Jy}$ could lie at $z > 4$. To ensure that optical follow-up is confined to a reasonable number of objects requires more selective criteria than just a simple radio flux limit.

We chose additional selection criteria which took into account the characteristics often seen in very distant radio galaxies namely, small angular size θ and steep radio spectral index α [e.g., McCarthy (1993)]. This latter criterion has been used extensively by a number of groups [e.g., Chambers, Miley & van Breugel (1990); Röttgering et al. (1994); Rhee et al. (1996); Chambers et al. (1997)]. Our chosen selection criteria were $\theta < 15''$ and $\alpha > 0.981$. Note that these criteria are imperfect in two ways: first, they are unlikely to filter out all the low-redshift objects, and second, they will exclude at least some high-redshift objects.

This second imperfection has a more profound impact on the aims of our project, so to examine the extent to which the spectral index and angular size cut-offs contribute to this we compared the angular sizes and spectral indices of the known $z > 3$ objects, with those of the most radio-luminous 3C sources (see Fig. 2). Many, but not all, high- z radio galaxies have

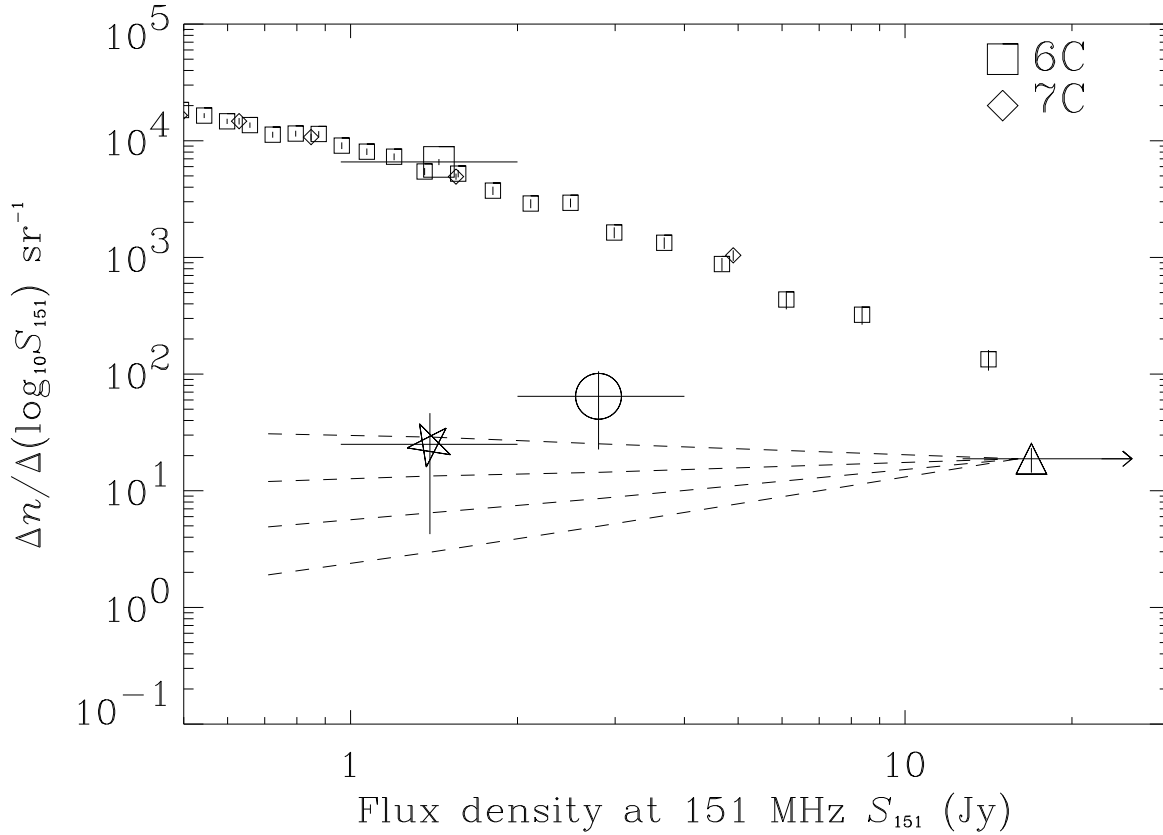


Figure 1. Predicted areal density of high-redshift radio sources as a function of 151-MHz flux density S_{151} and in comparison with the total source count; the source count is reproduced from Hales, Baldwin & Warner (1988) for 6C (squares) and from McGilchrist et al. (1990) for 7C (diamonds). The largest 6C symbol shows the source count for the 6C* sample discussed in this paper. The lowest 3 symbols represent measurements of the number of high radio luminosity ($28.0 < \log_{10} L_{151} < 28.7$) sources in three samples: represented by a triangle are (i) the 20 radio sources, galaxies plus quasars, with $z > 1.3$ in the revised 3CR sample (Laing et al. 1983); by an open circle the two sources, both galaxies, with $z > 3$ in the 6C sample (Eales et al. 1997); and by an open 5-pointed star the one radio galaxy at $z > 4$ found in a preliminary analysis of the 6C* sample (Rawlings et al. 1996). The horizontal bars show the S_{151} range of each sample, and the vertical bars are 68% confidence intervals calculated by adopting a Jeffreys' prior for the the probability density function of the areal density and by assuming a Poisson likelihood function for the number of high- L_{151} objects in each sample (see Sivia 1996); note in the case of 6C* that the true areal density may be systematically higher if the α and θ filtering has led to the exclusion of some high redshift objects. The dashed lines show the results of a crude but, for illustrative purposes, adequate model of the high- z evolution of the radio luminosity function: we parameterise this by $\rho \propto \rho_0 \times (1+z)^{-\gamma} \times L_{151}^{-\beta}$, set $\beta = 2$ (following Dunlop & Peacock 1990), and fix ρ to reproduce the 3C data at $z > 1.3$; the dashed lines show (from top to bottom) the effects of increasing γ from 0 to 3.

concave radio spectra like Cyg A, so the k -correction means that an $\alpha > 1$ criterion should exclude only a minority of the $z > 3$ objects. For the illustrative example depicted in Fig. 2, 35% of 3C objects redshifted to $z = 3$ or $z = 4$ would be excluded by our chosen spectral index criterion, while 29% would be excluded by the same criterion if they were redshifted to $z = 5$. Note, also that there are significant selection effects in the positioning of the known $z > 3$ radio galaxies in Fig. 2: most of these objects (represented by the open circles) have been selected as candidate high- z radio galaxies on the basis of their steep spectra, and

in some cases account has been taken of their small angular size.

We considered, but rejected, the possibility of using spectral curvature as an additional radio selection criterion [e.g., Lacy et al. (1994)]: although this might have improved the efficiency of our search for high- z galaxies, it would certainly have been a further cause of incompleteness. A clear demonstration of this is provided by the comparison in Fig. 3 of the radio spectra of the two highest redshift radio galaxies found to date in the 6C* sample: these objects, 6C 0140+326 with $z = 4.41$ and 6C 0032+412 with $z = 3.67$, have similarly steep values of α (and appear very close to

one another in Fig. 2) but in one case (6C 0140+326) there is obvious spectral curvature, whereas in the other a single straight power law provides an excellent fit over the full range of the available data. We quantify these considerations via the spectral fitting described in Section 3.1. Spectral curvature, although common, is thus not a ubiquitous feature of the radio spectra of $z \sim 4$ radio galaxies despite the high rest-frame frequencies probed (up to 40 GHz in the case of 6C 0032+412). This is perhaps not entirely surprising: the ‘leaky reservoir’ model for radio hotspots (e.g. Eales, Alexander & Duncan 1989) predicts that spectral curvature arises because of breaks at the extreme ends of the spectrum ($\lesssim 0.1$ GHz and $\gtrsim 10$ GHz; see also Chambers et al. 1990). The break values in a given $z \sim 4$ source can perfectly plausibly fall outside the rest-frame frequency range spanned by the common radio surveys, namely ≈ 0.75 –25 GHz; note also that there is empirical evidence for an upper break frequency $\gtrsim 400$ GHz in the hotspots of Cyg A (Eales et al. 1989).

For the example shown in Fig. 2, a naive calculation would imply that 50% of the 3C objects would be excluded by our angular size cut if they were redshifted to $z = 3$, 44% if redshifted to $z = 4$ and 32% if redshifted to $z = 5$. However, this simple calculation ignores any negative evolution of linear size with z . Statistically speaking there is good evidence for just such an evolutionary trend (e.g., Neeser et al. 1995; Blundell et al., in prep.), but an intrinsic spread in θ means that at least some $\theta > 15$ arcsec sources are already known at $z > 3$ (Fig. 2).

The 6C* sample of 34 radio sources has already led to the detection of one radio galaxy (6C 0140+326) with $z = 4.41$ (Rawlings et al. 1996), and one (6C 0032+412) with $z = 3.67$ (Rawlings et al., in prep). The former was not the first radio galaxy to be found at $z > 4$ — this was 8C 1435+635 at $z = 4.25$ (Lacy et al. 1994) — but it is currently the most distant radio galaxy known. In this paper (hereafter Paper I) and a companion paper (Paper II) we will present full details of the 6C* sample. In Paper I we describe the sample selection criteria, present VLA radio maps of the objects in the sample, and tabulate various parameters of the radio sources including spectral information derived from a combination of survey and VLA data. In Paper II (Rawlings et al., in prep) we will describe optical spectroscopy and near-infrared imaging of these sources. B1950.0 co-ordinates are used, and the convention for spectral index (α) is that $S_\nu \propto \nu^{-\alpha}$, where S_ν is the flux density at frequency ν .

2 SAMPLE DEFINITION

This project commenced with criteria based on a preliminary version of part VI of the 6C survey of radio sources at 151 MHz (kindly supplied by S. Hales)

which includes the continuous zone of Right Ascension between $22^{\text{h}}35^{\text{m}}$ and $09^{\text{h}}05^{\text{m}}$, passing through 0^{h} , and the range of Declination between $+30^\circ$ and $+51^\circ$. A patch of sky ~ 0.1 sr was chosen as the minimum size necessary to allow a reasonable chance of finding a $z > 4$ radio galaxy (see Fig. 1), and the choice of location of this patch was determined by two considerations: first, avoidance of the galactic plane (see Fig. 4); and second, a time allocation on an optical telescope suited to observations near $1^{\text{h}}30^{\text{m}}$ R.A. at northern declinations.

In this patch of sky all sources with S_{151} less than 1.00 Jy (according to the preliminary flux scales of the 6C catalogue) or greater than 2.00 Jy were rejected. Spectral indices of the remaining objects were found by obtaining positional coincidences (within $120''$) of sources in the 6C-VI catalogue and those in the 87GB catalogue of radio sources, the latter resulting from a survey at 4.85 GHz (Gregory & Condon 1991). Any object with a spectral index between 151 MHz and 4.85 GHz (i.e., $\alpha_{151\text{M}}^{4.85\text{G}}$) which was less than 1.0 was then rejected. Sources which met the flux density criterion for the 6C-VI survey but which were not detected in the 87GB survey were retained in the sample since such sources (if real) would inevitably have spectra steeper than this threshold.

The sources which were remaining were then cross-correlated* with those in the Texas Survey at 365 MHz (Douglas et al. 1996). Sources with entries in both the 6C-VI and the Texas surveys whose positions were coincident within $120''$ were only retained in the sample if their angular size as listed in the Texas survey (θ_{Texas}) was less than $15''$. This set of sources is henceforth denoted (6C-T-C). Those 6C sources with entries in the Texas survey but not in the 87GB survey were classed as 6C-T-C.

We were concerned to ensure we would not exclude an object whose size was $\lesssim 15''$ and whose two hotspots had sufficiently asymmetric spectra that the hotspot which dominated the overall source flux density at the frequency of one survey was different from the hotspot dominating at the frequency of a different survey. The worst case positional uncertainty (combining the uncertainties in quadrature) is $25''$. We experimented using somewhat over a 3σ tolerance for positional uncertainty of $90''$ and found there was no

* The searches were made for *all* matches in the Texas and in the 87GB samples within a $120''$ search radius. There were 3 cases of more than one match to a 6C object being found, each of these arising from a double entry in the Texas catalogue. These 3 examples were in each case 2 objects with fluxes differing by not more than 50 mJy (i.e., $< 2\sigma$) and separated by not more than 5 arcsec. We used the nearer of the two matches to the 6C position in each case, which also happened to be in each case the match with the lower flux density. For details on where this occurred, please see ‘Notes on Individual Sources’ — Section 4.

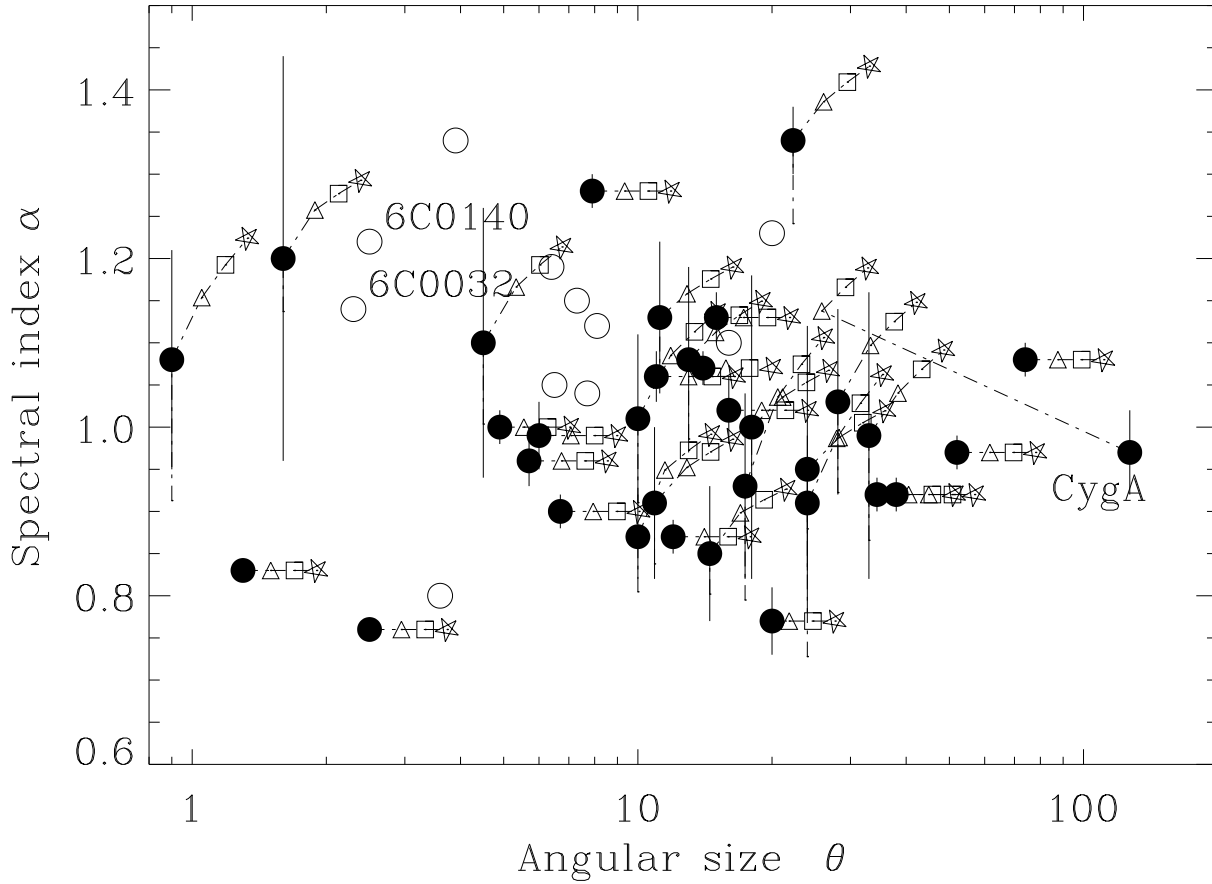


Figure 2. The radio spectral index α (evaluated at 1 GHz as described in Section 3.1), angular size θ (in arcsec) plane for 3C radio galaxies (filled circles, Cyg A marked) and the $z > 3$ radio galaxies known prior to submission of this paper (open circles, 6C0032+412 & 6C0140+326 marked). For the 3C sources we have used their integrated radio spectra (taken from Laing & Peacock 1980) and observed angular sizes to predict the loci of similar radio sources at $z = 3$ (triangles), $z = 4$ (squares) and $z = 5$ (stars).

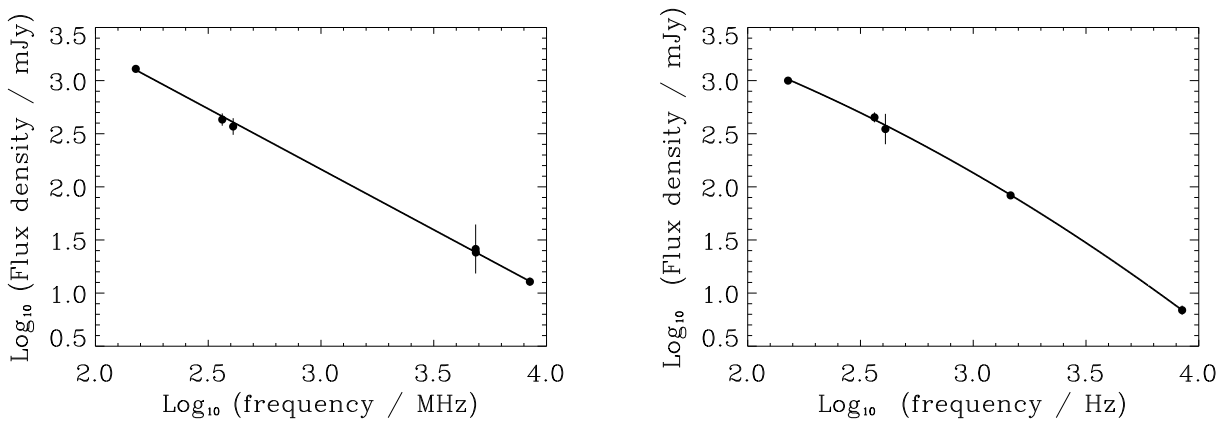


Figure 3. These plots show the flux densities against frequency for two high redshift radio galaxies: *left*: 6C0032+412 at $z = 3.67$ and *right*: 6C0140+326 at $z = 4.41$. In the case of 6C0032+412 the fit shown is a straight line while for 6C0140+326 a curvature is required as described in the text.

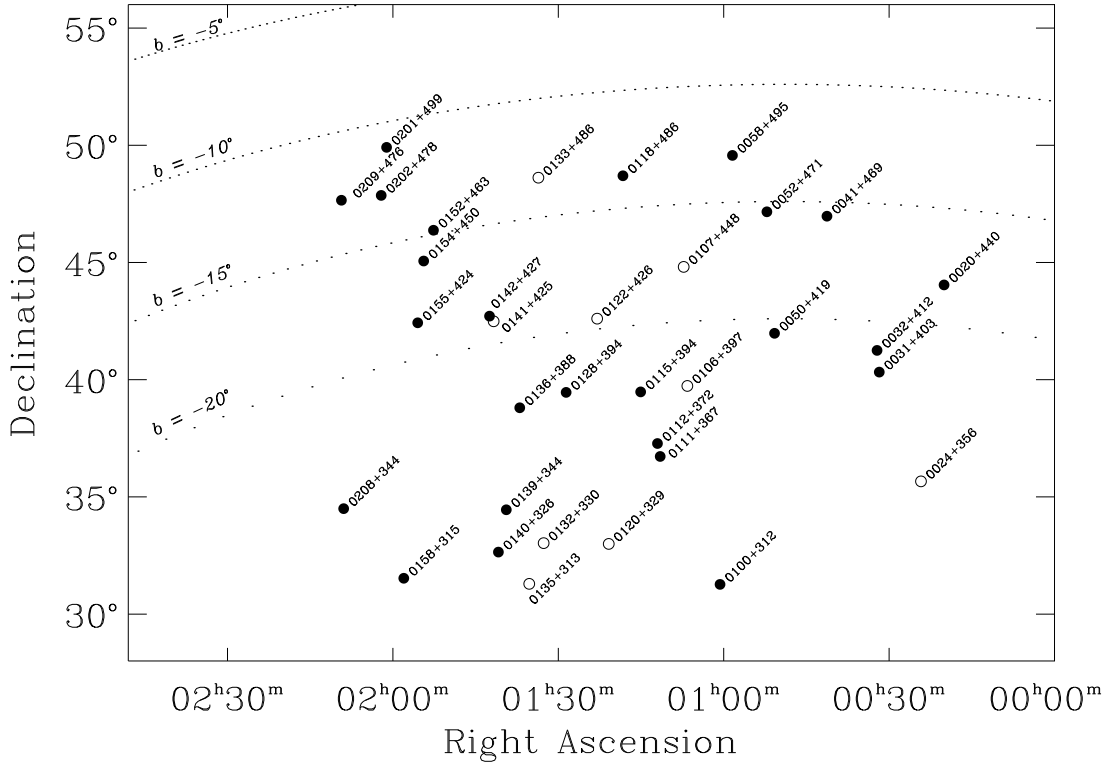


Figure 4. The sky locations of the members of the 6C* sample; we have discriminated between objects in the preliminary version of the sample (filled symbols) and those only in the final version (open symbols). Lines of constant galactic latitude (b) are plotted as dotted lines.

difference if a very conservative search radius of $120''$ was employed. At the flux levels of these surveys there is a minimal risk of excluding an intrinsically steep spectrum source by spuriously matching it with an inverted-spectrum neighbour in the higher frequency survey since the areal density of these objects in these surveys is so low.

With these preliminary (sub-)samples established, an extensive series of multi-wavelength observations began. Radio maps were obtained with the VLA, enabling accurate positioning and orientation of slits for spectroscopy.

We reviewed the selection criteria and sample membership once the final version of the 6C catalogue became available in this region (Hales et al. 1993). All of the final catalogue analysis and manipulation was carried out using the Starlink Cursa Project software written by Clive Davenhall. It was found that all objects for which optical and infra-red follow-up had occurred were selected by imposing the flux limits $0.96 \text{ Jy} \leq S_{151} \leq 2.00 \text{ Jy}$, and a radio spectral index limit $\alpha_{151\text{M}}^{4.85\text{G}} \geq 0.981$.

In this final version of our 6C* sample we in-

cluded those 6C sources with no entry in the Texas catalogue (within $120''$) nor in the 87GB survey (within $120''$) and denoted these as 6C- $\bar{\text{T}}-\bar{\text{C}}$ since it was plausible that such sources have very steep spectra.[†] We also retained those 6C sources in the 87GB survey but not in the Texas survey and named this sub-set as 6C- $\bar{\text{T}}-\text{C}$.

The final selection criteria may thus be summarised as follows:

- $00^{\text{h}}20^{\text{m}} \leq \text{R.A.} \leq 02^{\text{h}}10^{\text{m}}$
- $30^{\circ} \leq \text{Dec.} \leq 51^{\circ}$
- $0.96 \text{ Jy} \leq S_{151} \leq 2.00 \text{ Jy}$
- $\alpha_{151\text{M}}^{4.85\text{G}} \geq 0.981$, where calculable.
- $\theta_{\text{Texas}} < 15''$, where available.

The final 6C* sample comprises 34 objects. Of these 9 were missing from our original version of the sample (marked by asterisks in Table 1 and see also

[†] Three objects in this subset were found to be not appropriate members of the sample after inspection of the 6C radio maps and consideration of other data — see Section 6.

Fig. 4). The only systematic difference between the original and final versions of the sample lies in the inclusion of the 4 sources in the 6C- \overline{T} - \overline{C} sub-sample. The remaining 5 objects were not part of the original sample because of changes in the finalised 6C survey, and because of inadvertent omission in a process which was not fully automated.

The effects of the θ and α selection criteria on the original flux-limited sample are illustrated in Fig. 5: about 12 per cent of the original flux-limited sample were retained once these filtering criteria were applied. Only one of the objects matched in the Texas survey and retained in the final sample was deemed by this survey to have a size other than unresolved. This object is 6C 0133+486 whose angular size, deemed by the Texas survey to be $10''$, turned out to be $10.9''$. One of the multiply-matched objects (6C 0031+403) had one match with a purported angular size of $23''$ but a nearer match deemed to be unresolved. We measured a size of $\approx 20''$ for this object.

The sky area of the 6C* survey is 0.133 sr. The radio flux density measurements of the sample members obtained from the various radio surveys are compiled in Table 1. One final complication concerns the slightly discrepant 151 MHz source count in this region of the 6C survey (Fig. 1) but this effect is at the level where it is plausibly a statistical fluctuation.

3 RADIO OBSERVATIONS

Radio observations of the sources were made using the VLA in various configurations, details of which are tabulated in Table 2. In each case, the bandwidth was 50 MHz (except for the 1.5 GHz observations in 1995/1996 where a bandwidth of 25 MHz was used). The primary flux calibrators used were either 3C 286 or 3C 48, and the flux scale used in each case was the then most recently determined for the VLA. We calibrated and reduced the data using standard procedures in *AIPS*, including self-calibration for phase only, where there was sufficient signal-to-noise.

We present maps in Figures 6 — 11; lowest contour levels, beam sizes and other relevant data are tabulated in Table 3. For each map presented, adjacent contour levels differ from one another by a factor of $\sqrt{2}$ in flux density. The exact observing frequencies used were: L-band 1.4649 GHz, C-band 4.8601 GHz and X-band 8.4399 GHz.

3.1 Spectral fitting

With regard to radio spectral index α the sample was selected on the basis of a two frequency (151 MHz and 4850 MHz) criterion, namely, $\alpha_{151M}^{4.85G} > 0.981$. More sophisticated fitting of the radio spectra was made possible by consideration of data from many radio surveys (Table 1), and furthermore in combination with data from our VLA mapping. We fit-

ted the flux density data using a Bayesian polynomial regression analysis which assessed the posterior probability density function (PDF) for the required order of a polynomial fit (Gull 1988; Sivia 1996); we chose $x = \log_{10}(\nu/\text{MHz})$ as the dependent variable and expanded the independent variable $y = \log_{10} S_\nu = \sum_{r=0}^N a_r x^r$. In most cases the peak in the PDF led us to prefer a first-order polynomial, and the slope of the fit ($-a_1$) evaluated to give α_{1000} for the survey data or α_{VLA} for the full radio dataset. In some cases the PDF led us to prefer a second-order fit, implying significant curvature in the radio spectrum: in these cases we calculated the curvature $\beta = -2a_2$, and α_{1000} (or α_{VLA}) as the slope evaluated at 1 GHz, namely $-a_1 + 6\beta$. In no case was a higher order fit preferred. In the cases of significant spectral curvature there are often fairly large errors in the values of α_{1000} and α_{VLA} .

4 NOTES ON INDIVIDUAL SOURCES

6C 0020+440 Comparison of radio maps at 1.5 and 8.4 GHz show that both lobes have steep spectra ($\alpha \gtrsim 1.0$).

6C 0024+356 We only have a map of this object at 8.4 GHz but both components have the resolved appearance of lobes and/or hotspots and there is no evidence of a core between them.

6C 0031+403 The core position in Table 2 is from the 8.4 GHz map, where it is clearly the dominant component, implying a spectral index ~ 0 . The diffuse lobes to the south-east and west of the core are also detected at 8.4 GHz. This object was found to have 2 matches in the Texas catalogue, which are separated from one another by 4.7 arcseconds and fluxes which are 432 and 480 mJy.

6C 0032+412 The core position in Table 2 is from the 4.9 GHz map shown in Fig. 6; the core has a spectral index ~ 0 (Rawlings et al. in prep.).

6C 0041+469 The core position in Table 2 is of the weak unresolved component in the 4.9 GHz map shown in Fig. 6 although the resolution of the 8.4 GHz map is too low to allow measurement of the spectral index.

6C 0050+419 The position given in Table 2 is the peak of the component seen in Fig. 6 which appears to be marginally resolved approximately along p.a. 15° . There is some evidence for another component in the 8.4 GHz map at 00 50 46.12 +41 58 37.52. The structure of this radio source and the search position for any optical identification are therefore uncertain.

6C 0052+471 Both components shown in the 1.5 GHz map in Fig. 7 have steep spectra ($\alpha \gtrsim 1.0$).

6C 0058+495 Both components shown in the 4.9 GHz map in Fig. 7 have steep spectra ($\alpha \sim 1.0$). This object was found to have 2 matches in the Texas catalogue, which are separated from one another by 2.2 arcseconds and fluxes which are 420 and 444 mJy.

Source	$\alpha_{151M}^{4.85G}$	α_{1000}	6C 151 MHz	Texas 365 MHz	B2/3 408 MHz	WB 1400 MHz	87GB 4850 MHz
6C-T-C							
6C 0020+440	1.13 ± 0.10	1.13 ± 0.03	2000 ± 45	697 ± 23	700 ± 36	178 ± 30	40 ± 6
6C 0031+403	0.99 ± 0.13	0.95 ± 0.03	960 ± 45	432 ± 28	390 ± 30	138 ± 30	31 ± 6
6C 0032+412	1.13 ± 0.15	1.19 ± 0.03	1290 ± 45	430 ± 25	370 ± 29	-	26 ± 6
6C 0050+419	1.01 ± 0.13	1.02 ± 0.01	1000 ± 45	396 ± 19	370 ± 29	-	30 ± 6
6C 0052+471	1.00 ± 0.10	1.00 ± 0.03	1310 ± 45	561 ± 22	-	100 ± 30	41 ± 6
6C 0058+495	1.02 ± 0.12	1.00 ± 0.02	970 ± 45	420 ± 29	-	-	28 ± 5
6C 0111+367	1.00 ± 0.12	0.96 ± 0.04	1110 ± 45	511 ± 21	390 ± 50	-	34 ± 6
6C 0128+394	0.99 ± 0.09	1.06 ± 0.41^c	1940 ± 45	1111 ± 20	920 ± 40	261 ± 30	62 ± 9
6C 0133+486*	1.06 ± 0.09	1.08 ± 0.02	1890 ± 45	685 ± 36	-	169 ± 30	48 ± 7
6C 0139+344	1.05 ± 0.14	1.09 ± 0.16	1100 ± 45	589 ± 22	570 ± 60	-	29 ± 6
6C 0152+463	1.02 ± 0.10	1.01 ± 0.04	1290 ± 45	493 ± 20	530 ± 33	145 ± 30	38 ± 6
6C 0154+450	1.02 ± 0.12	1.08 ± 0.07	1150 ± 45	357 ± 25	380 ± 30	-	34 ± 6
6C 0155+424	1.06 ± 0.10	1.06 ± 0.01	1510 ± 45	593 ± 20	520 ± 33	143 ± 30	38 ± 6
6C 0158+315	1.03 ± 0.12	0.88 ± 0.07	1510 ± 45	808 ± 30	710 ± 80	197 ± 30	43 ± 8
6C-T- \bar{C}							
6C 0024+356*	> 1.09	1.12 ± 0.20	1090 ± 45	515 ± 19	-	-	-
6C 0100+312	> 1.11	$1.68 \pm 0.14^\dagger$	1160 ± 45	$^\ddagger 223 \pm 27$	290 ± 50	-	-
6C 0107+448*	> 1.07	1.50 ± 0.07	1040 ± 45	258 ± 19	260 ± 26	-	-
6C 0112+372	> 1.07	1.11 ± 0.08	1030 ± 45	502 ± 18	370 ± 29	-	-
6C 0115+394	> 1.05	1.12 ± 0.05	960 ± 45	369 ± 20	290 ± 28	-	-
6C 0118+486	> 1.06	1.22 ± 0.20	980 ± 45	333 ± 21	-	-	-
6C 0122+426*	> 1.08	1.09 ± 0.08	1050 ± 45	451 ± 23	460 ± 31	182 ± 30	-
6C 0136+388	> 1.06	1.10 ± 0.07	990 ± 45	478 ± 20	360 ± 29	-	-
6C 0140+326	> 1.06	1.11 ± 0.05	1000 ± 45	451 ± 21	350 ± 50	-	-
6C 0142+427	> 1.17	1.21 ± 0.12	1460 ± 45	448 ± 20	530 ± 33	-	-
6C 0201+499	> 1.10	1.05 ± 0.16	1140 ± 45	450 ± 21	-	-	-
6C 0201+478	> 1.08	1.22 ± 0.19	1060 ± 45	362 ± 21	-	-	-
6C 0208+344	> 1.05	1.05 ± 0.08	970 ± 19	471 ± 19	-	-	-
6C 0209+476	> 1.10	1.13 ± 0.08	1140 ± 45	526 ± 19	-	-	-
6C- \bar{T} -C							
6C 0041+469	1.07 ± 0.12	0.98 ± 0.06	1530 ± 45	-	650 ± 35	-	38 ± 7
6C 0141+425*	1.06 ± 0.11	0.95 ± 0.07	1640 ± 45	-	(see notes)	265 ± 30	41 ± 7
6C- \bar{T} - \bar{C}							
6C 0106+397*	> 1.05	1.08 ± 0.30	960 ± 45	-	460 ± 31	-	-
6C 0120+329*	> 1.24	> 1.24	1870 ± 45	-	-	(see notes)	-
6C 0132+330*	> 1.19	> 1.19	1560 ± 45	-	-	-	-
6C 0135+313*	> 1.12	> 1.12	1240 ± 45	-	-	-	-

Table 1. The survey flux densities of the 6C* sources in mJy and spectral indices derived from these. The first column gives the source name, with an asterisk indicating if the source had been excluded from the preliminary version of the sample. The second column lists the spectral index α derived from the 6C and 87GB flux densities, i.e., the value used in the selection criterion for sample membership. The third column lists the spectral index at 1000 MHz derived from the fitting procedure described in the Section 3.1; the fit requiring spectral curvature is marked with a ‘c’, and values for the curvature β for this object, 6C 0128+394, is 0.64. The remaining columns give survey flux densities, properties of these surveys are: 6C, a 151-MHz survey with a resolution of ≈ 4 arcmin (e.g., Hales et al. 1988), the numbers listed are fitted peak flux densities; Texas, a 365-MHz survey with a complicated beam meaning that the flux densities of sources larger than a few arcmin are unreliable (Douglas et al. 1996); B2.1, B2.3 and B3, the Bologna 408-MHz B2.1 (Colla et al. 1970), B2.3 (Colla et al. 1974) and B3 (Ficarra, Grueff & Tomassetti 1985) surveys with resolutions of $\lesssim 10$ arcmin and $\lesssim 5$ arcmin for the B3 survey (B3 is used except in the cases of 6C 0100+312, 6C 0140+326 and 6C 0158+315 [B2.1] and in the cases of 6C 0111+367, 6C 0139+344 [B2.3]); WB, data compiled by White & Becker (1992) from the 1400-MHz survey of Condon & Broderick (1986) which had a resolution of ≈ 12 arcmin; 87GB, a 4850-MHz survey with a resolution of ≈ 3.5 arcmin (Gregory & Condon 1991). The \dagger symbol indicates that the spectral index is unreliable because the flux density marked with a \ddagger is possibly underestimated because of the large angular size of the radio source. The errors in 6C fluxes were obtained following the assumption in Hales et al. (1993; 6C-VI) that the errors in this survey are 50% worse than in Baldwin et al. (1985; 6C-I) — thus we take 45 mJy as the typical error in a flux density measurement from 6C. ~~© 0000 RAS, MNRAS 000, 000–000~~ WB and 87GB flux density measurements were either taken from the catalogues, or estimated from the noise statistics of the survey.

Source	R.A. B1950.0	Dec. B1950.0	Position flag	Shape	Angular size	VLA-L 1.5 GHz	VLA-C 4.9 GHz	VLA-X 8.4 GHz	Source
6C 0020+440	00 20 01.71	+44 02 32.3	h	c	10.0	L1-A		X1-C	6C 0020+440
6C 0024+356	00 24 12.89	+35 39 47.7	h	c	9.6			X3-BnA	6C 0024+356
6C 0031+403	00 31 46.79	+40 19 26.3	c	dt	≈ 20	L1-A		X1-C	6C 0031+403
6C 0032+412	00 32 10.73	+41 15 00.2	c	t	2.3		C1-A	X1-C	6C 0032+412
6C 0041+469	00 41 16.04	+46 58 27.2	c?	t?	3.8		C1-A	X1-C	6C 0041+469
6C 0050+419	00 50 46.52	+41 58 45.3	p	a	< 0.5		C1-A	X1-C	6C 0050+419
6C 0052+471	00 52 09.59	+47 09 46.2	h	c	5.6	L1-A		X1-C	6C 0052+471
6C 0058+495	00 58 24.75	+49 34 04.3	h	c	3.2		C1-A	X1-C	6C 0058+495
6C 0100+312	01 00 39.71	+31 16 06.5	c	t	89.7	L1-A		X1-C	6C 0100+312
6C 0106+397	01 06 35.31	+39 44 02.8	h	c	3.0	L2-A			6C 0106+397
6C 0107+448	01 07 15.42	+44 48 44.5	c?	dt?	5.8			X2-BnA	6C 0107+448
6C 0111+367	01 11 30.99	+36 43 32.8	p	a	1.2		C1-A	X1-C	6C 0111+367
6C 0112+372	01 12 00.33	+37 16 41.4	c	t?	3.6		C1-A	X1-C	6C 0112+372
6C 0115+394	01 15 03.47	+39 28 45.9	c	t	7.7			X3-BnA	6C 0115+394
6C 0118+486	01 18 16.49	+48 41 58.0	c?	t?	16.1	L1-A		X1-C	6C 0118+486
6C 0120+329 [‡]	01 20 50.7	+32 59 45	g	dt	130.0	L2-A			6C 0120+329
6C 0122+426	01 22 56.80	+42 36 16.0	h	c	0.9			X2-BnA	6C 0122+426
6C 0128+394	01 28 34.67	+39 27 32.0	h	c	2.6			X3-BnA	6C 0128+394
6C 0132+330	01 32 39.22	+33 01 42.0	p	u	< 8			X4-DnC	6C 0132+330
6C 0133+486	01 33 36.58	+48 37 04.0	h	c	10.9			X3-BnA	6C 0133+486
6C 0135+313	01 35 16.13	+31 17 27.3	p	a	1.8	L2-A			6C 0135+313
6C 0136+388	01 36 59.09	+38 48 09.2	c	dt	4.2		C1-A	X1-C	6C 0136+388
6C 0139+344	01 39 25.87	+34 27 02.5	c?	t?	6.5		C1-A	X1-C	6C 0139+344
6C 0140+326	01 40 51.53	+32 38 45.8	h	c	2.5	L1-A		X2-BnA	6C 0140+326
6C 0141+425	01 41 42.00	+42 29 15.5	h	d?	113?			X4-DnC	6C 0141+415
6C 0142+427	01 42 28.13	+42 42 41.6	c	t	15.2	L1-A		X1-C	6C 0142+427
6C 0152+463	01 52 38.22	+46 22 30.4	c?	dt?	5.7	L3-BnA	C1-A	X1-C	6C 0152+463
6C 0154+450	01 54 24.85	+45 03 46.4	c	t	21.6			X1-C	6C 0154+450
6C 0155+424	01 55 29.74	+42 25 38.0	p	a	4.0	L3-BnA		X1-C	6C 0155+424
6C 0158+315	01 58 01.53	+31 31 47.0	p	a	1?		C1-A	X1-C	6C 0158+315
6C 0201+499	02 01 08.41	+49 54 38.1	h	c	0.9		C1-A	X1-C	6C 0201+499
6C 0202+478	02 02 07.03	+47 51 42.2	h	c	16.5	L1-A		X1-C	6C 0202+478
6C 0208+344	02 08 55.47	+34 29 57.3	h	c	2.2		C1-A	X1-C	6C 0208+344
6C 0209+476	02 09 20.01	+47 39 16.5	p	u	< 0.5		C1-A	X1-C	6C 0209+476

Table 2. Table summarising our snapshot observations with the VLA. The positions of the objects are indicated in columns 2 & 3; the positions were measured from the radio core if present (this is denoted ‘c’ in column 4), or the peak of the source if unresolved or amorphous (use of these methods are denoted ‘p’ in column 4), or in the case of a classical double by taking the mid-point of the hotspot peaks (use of this method is denoted ‘h’ in column 4). The structures of each object as inferred from inspection of the VLA maps are indicated in column 5 as follows: u: unresolved, c: classical double, t: classical triple, a: amorphous/partially resolved; a ‘d’ preceding ‘c’ or ‘t’ indicates significant distortion in the structure. Largest angular sizes (or separation of the hotspots for the classical doubles) are indicated in column 5; the units are arcseconds. [‡]For this source the position and structure are quoted from de Ruiter et al. (1986) — the ‘g’ in column 4 indicates that the position given is that of the galaxy identification. Observations we made using the VLA at 1.5, 4.9 and 8.4 GHz are denoted by the letters L, C, and X respectively followed by a number referring to the date on which the observations were made. Data presented as maps in this paper are indicated by bold type. The codes are as follows: X1-C: 1990 November 8, C-array. C1-A: 1991 August 4, A-array. L1-A: 1991 August 2, A-array. L2-A: 1995 July 29, A-array. X2-BnA: 1995 September 25, BnA-array. X3-BnA: 1995 September 27, BnA-array. L3-BnA: 1995 September 27, BnA-array. L4-DnC: 1996 May 21, DnC-array. X4-DnC: 1996 May 21, DnC-array.

Source name	Beam FWHM	Peak flux	Lowest contour	VLA L 1.5 GHz	VLA C 4.9 GHz	VLA X 8.4 GHz	α_{VLA}
6C 0020+440	1.40 ²	99.58	1.00	166.4 ± 3.3		21.0 ± 0.7	1.12 ± 0.02
6C 0024+356	0.71 × 0.59 p.a. 112°	2.12	0.25			18.1 ± 0.6	1.04 ± 0.02
6C 0031+403	1.40 ²	16.31	0.88	> 134.8 ± 4.7		48.8 ± 1.0*	0.87 ± 0.03
6C 0032+412	0.50 ²	13.27	0.35	79.9 ± 2.4†	24.1 ± 0.4	12.8 ± 0.5	1.14 ± 0.01
6C 0041+469	0.45 ²	9.00	0.60		35.2 ± 1.5	17.3 ± 0.6	1.11 ± 0.02 ^c
6C 0050+419	0.50 ²	7.53	0.50		19.7 ± 0.8	14.6 ± 0.6	1.09 ± 0.03
6C 0052+471	1.45 ²	48.97	1.20	145.1 ± 5.5		24.1 ± 0.8	0.99 ± 0.01
6C 0058+495	0.45 ²	18.98	0.55		36.3 ± 1.1	19.2 ± 0.7	0.96 ± 0.02
6C 0100+312	1.25 ²	14.22	0.40	> 49.6 ± 0.7‡		> 16.6 ± 1.1*	1.39 ± 0.20
6C 0106+397	1.86 × 1.41 p.a. 55°	81.85	1.00	145.9 ± 1.5			1.10 ± 0.16 ^c
6C 0107+448	1.12 × 0.97 p.a. 2°	1.34	0.20			> 4.5 ± 0.4	1.35 ± 0.03
6C 0111+367	0.40 ²	14.70	0.50		31.8 ± 1.1	20.3 ± 0.7	1.02 ± 0.02
6C 0112+372	0.45 ²	4.05	0.50		14.2 ± 1.1	7.8 ± 0.4*	1.21 ± 0.58 ^c
6C 0115+394	0.72 × 0.60 p.a. -87°	2.00	0.25			> 8.7 ± 0.5*	1.17 ± 0.01
6C 0118+486	1.50 ²	24.94	0.80	70.1 ± 3.1		12.4 ± 1.1*	1.09 ± 0.02
6C 0122+426	0.71 × 0.60 p.a. 59°	8.02	0.25			12.1 ± 0.3	1.09 ± 0.53 ^c
6C 0128+394	0.75 × 0.57 p.a. 51°	19.85	0.30			43.5 ± 0.5	0.93 ± 0.27 ^c
6C 0132+330	7.55 × 6.12 p.a. 71°	8.80	0.30			9.3 ± 0.3	1.27 ± 0.03
6C 0133+486	0.78 × 0.57 p.a. 50°	3.69	0.30			> 6.1 ± 0.5‡	^d
6C 0135+313	1.63 × 1.19 p.a. 86°	43.07	0.40	83.4 ± 0.6			1.19 ± 0.04
6C 0136+388	0.45 ²	32.03	0.50		23.4 ± 1.1	9.4 ± 0.6	1.12 ± 0.38 ^c
6C 0139+344	0.50 ²	11.55	0.40		> 34.4 ± 1.6	17.4 ± 0.8	1.02 ± 0.21 ^c
6C 0140+326	1.30 ²	41.76	0.80	83.1 ± 1.1	17.1 ± 0.5†	6.9 ± 0.3	1.22 ± 0.12 ^c
6C 0141+425	7.21 × 5.89 p.a. 85°	0.81	0.40			> 3.4 ± 0.6*	^d
6C 0142+427	1.45 ²	25.58	1.00	117.9 ± 2.3		20.7 ± 1.0	1.07 ± 0.03
6C 0152+463	0.50 ²	14.43	0.50	144.7 ± 0.4	43.4 ± 0.9	22.5 ± 0.6	0.99 ± 0.02
6C 0154+450	2.44 × 2.07 p.a. 42°	8.36	0.40			20.0 ± 1.0	1.00 ± 0.03
6C 0155+424	4.19 × 1.56 p.a. 87°	51.71	0.30	163.5 ± 0.5		27.5 ± 0.7	0.99 ± 0.02
6C 0158+315	0.50 ²	38.93	0.30		49.8 ± 0.6	28.2 ± 0.6	1.00 ± 0.02
6C 0201+499	0.47 × 0.42 p.a. -36°	21.19	0.30		25.1 ± 0.5	10.8 ± 0.6	1.10 ± 0.01
6C 0202+478	1.29 × 1.13 p.a. 18°	43.22	0.80	85.0 ± 2.2		7.7 ± 1.0	1.10 ± 0.02
6C 0208+344	0.45 × 0.43 p.a. 30°	18.34	0.30		28.8 ± 0.6	13.7 ± 0.8	1.02 ± 0.03 ^c
6C 0209+276	0.47 × 0.42 p.a. -38°	18.13	0.30		25.8 ± 0.4	12.1 ± 0.6	1.12 ± 0.03 ^c

Table 3. The columns in this table are from left to right: source name, FWHM (in arcseconds) of the synthesized beam of the radio maps (Figures 6 — 11) and position angle of its major axis if non-circular, peak flux density (in mJy/beam), lowest contour (in mJy/beam) on the maps shown, integrated flux densities measured from all our maps given in mJy. The right-most column contains the slope of $\log(\text{flux}) - \log(\text{frequency})$ data evaluated at 1 GHz (see Section 3.1 for details). The † symbol means that the flux density is from observations in the literature at a nearby frequency: MERLIN 1658 MHz data in the case of 6C 0032+412 (Rawlings et al., in prep.); VLA 4885 MHz data in the case of 6C 0140+426 (Rawlings et al. 1996). The ‡ symbol means that the integrated flux should be considered a lower limit since spectral fitting implies that some of the source flux has not been sampled by the shortest VLA baselines used for the observation, while a > implies that on the basis of angular size considerations, there is a possibility that the flux has been undersampled. An asterisk means that a flat-spectrum core contributes significantly to the total flux at this frequency. A ‘c’ means that spectral curvature is required by the flux data: the values of β (see Section 3.1 for definition) are 0.33 (6C 0041+469), 0.88 (6C 0106+397), 0.47 (6C 0112+372), 0.33 (6C 0122+426), 0.40 (6C 0128+394), 0.44 (6C 0136+388), 0.45 (6C 0139+344), 0.35 (6C 0140+326), 0.35 (6C 0208+344) and 0.38 (6C 0209+476). A ‘d’ means no useful additional spectral information is available as a result of the VLA imaging.

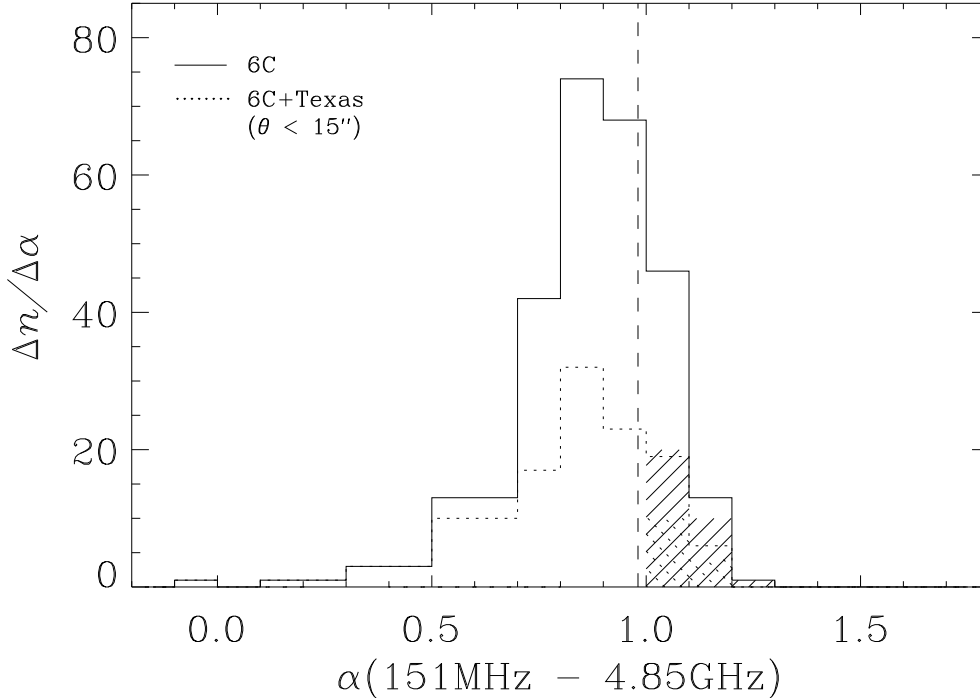


Figure 5. The solid line delineates the histogram of spectral indices between 151 MHz (from the 6C survey) and 4.85 GHz (from the 87GB survey) for those 279 6C objects satisfying the flux limits and sky area boundaries described in Section 2. Of these 279 objects, 248 have matches in the 87GB catalogue and their calculated spectral indices are used. The remaining 31 of these objects did not have matches (within $120''$) and so lower limits to their spectral indices were derived taking the upper limit for their flux density at 4.85 GHz to be 25 mJy (the flux limit to which the 87GB survey is complete). The vertical dashed line is plotted at the spectral index limit of 0.981. The hatched lines show the contributions from the lower limits to the spectral indices of objects without matches in the 87GB survey. The dotted line shows the histogram for those 112 objects in 6C which had a match in the Texas catalogue and whose angular size was quoted in this survey as being $< 15''$; for these objects which have matches in the 87GB catalogue, their calculated spectral indices between 151 MHz and 4.85 GHz are used, while for those 14 objects which do not have matches in the 87GB catalogue lower limits for spectral indices were derived assuming the same upper limit to flux density as previously, namely 25 mJy. The dotted hashed lines indicate the contribution from these 14 objects.

6C 0100+312 Note that the Texas flux density is likely to be an underestimate of the true value because of the size of source. The peak brightness of the core on the map shown in Fig. 7 is 4.7 ± 0.1 mJy/beam. The position in Table 2 is measured from the core seen in the 1.5 GHz map in Fig. 7; the core has a spectral index of ~ 0 .

6C 0106+397 Vigotti et al. (1989) find this object to be unresolved at 1.4 GHz with a flux density of 151 mJy. The radio spectrum of 6C 0106+397 between 151 and 1400 MHz requires extreme ($\beta = 0.88$) curvature at higher frequencies to be consistent with an assumed 25mJy limit from the 87GB survey.

6C 0107+448 The position given in Table 2 is of the eastern-most of the three brightest components shown in the map in Fig. 7. We have no spectral in-

formation to determine whether this feature is in fact a core.

6C 0111+367 Our 4.9 GHz map shows only the hotspot-like feature (with $\alpha \sim 1$) seen in Fig. 7; however, there are two additional very weak features on our 8.4 GHz map at $01\ 11\ 29.8\ +36\ 43\ 27.5$ (2.3σ) and $01\ 11\ 27.8\ +36\ 43\ 19$ (3.6σ) which together with the feature seen on the 4.9 GHz map are roughly colinear.

6C 0112+372 The position given in Table 2 is the position of the brightest component on the 4.9 GHz map in Fig. 8. This has a spectral index ~ 0 . An eastern lobe is detected both at 4.9 and 8.4 GHz but no corresponding emission to the west is seen in either band.

6C 0115+394 We have assumed that the component whose position is given in Table 2 is the core of a triple source although we have no measure of its spectral index. Vigotti et al. (1989) find this object to be unresolved at 1.4 GHz with a flux density of 88 mJy.

6C 0118+486 The position given in Table 2 is that of the middle component on the 1.5 GHz map in Fig. 8. The spectral index of this feature is ~ 0.5 . Both the northern and southern lobes are detected at 8.4 GHz and have spectral indices $\gtrsim 1.0$.

6C 0120+329 This is the only object in the sample for which we do not present a map because a better map is in de Ruiter et al. (1986). This source is associated with NGC507 and has a redshift of 0.0164.

6C 0122+426 From our single frequency data we are unable to ascertain whether the core is either of the features seen in Fig. 8. The 6C map is marginally resolved in the direction of a second B3 match at 01 23 02.3 42 40 06 (whose B3 flux density 130 mJy) but, with a separation of $4'$ from our VLA position, this is unlikely to contribute significantly to the peak 6C flux density.

6C 0128+394 We only have a map of this object at 8.4 GHz but both components have the resolved appearance of lobes and/or hotspots and there is no evidence of a core between them.

6C 0132+330 The 6C flux density of this source is highly uncertain because of its proximity to 3C 48.

6C 0133+486 We only have a map of this object at 8.4 GHz but the main features seen have the resolved appearance of lobes and/or hotspots.

6C 0135+313 Our 1.5 GHz map only partially resolves this source along p.a. 30° .

6C 0136+388 The brightest feature on the 4.9 GHz map in Fig. 8 has a spectral index ~ 0 and we take this to be the core. The lobe to the south-east is also seen at 8.4 GHz but at neither frequency is there evidence of a lobe to the north-west.

6C 0139+344 Both of the two main features on the 4.9 GHz map have spectral indices $\gtrsim 1$; the core position given is for the weak component between the main components on the 4.9 GHz map. Our 8.4 GHz map has insufficient resolution to confirm whether this is the core.

6C 0140+326 This $z = 4.41$ object is discussed in detail in Rawlings et al. (1996).

6C 0141+425 There are two sources in B3 at 01 41 46.5 42 29 43 with 408-MHz flux density 390 mJy and at 01 41 37.5 42 28 48.0, with 408-MHz flux density 410 mJy which are within the 6C beam. It is therefore plausible that this object is a $113''$ double. Our 8.4 GHz data in Fig. 9 detects only emission associated with the former B3 object and this emission appears to be resolved, consistent with it not being detected by the Texas survey. The low resolutions of the WB and 87GB surveys (listed in the caption to Table 1) mean that it is not possible to resolve emission separately from each of the components found in

B3. A further discussion of these and other data on this object will be found in Paper II.

6C 0142+427 The core position given in Table 2 is that of the feature closest to the centre of the map presented in Fig. 9 which also has the flattest spectrum ($\alpha \sim 0$).

6C 0152+463 The position given is that of the most easterly component on the 4.9 GHz map which is shown in Fig. 10. Our 1.5 and 8.4 GHz maps have insufficient resolution to confirm the identity of this feature as the core.

6C 0154+450 The position given in Table 2 is that of the middle component shown in the map in Fig. 10. We have no data at a second frequency.

6C 0155+424 This source is somewhat resolved along p.a. 80° .

6C 0158+315 Our 4.9 GHz data resolves this source, although it is unclear whether this is a hotspot of a larger source or a discrete object. This object was found to have 2 matches in the Texas catalogue, which are separated from one another by $1.3''$ and flux densities which are 834 and 808 mJy.

6C 0201+499 This source is most likely to be a small double.

6C 0202+478 Both components have spectral indices $\gtrsim 1$.

6C 0208+344 Neither of the components seen in the 4.9 GHz map in Fig. 10 has a spectral index which implies a core.

6C 0209+276 This object appears to be marginally resolved.

5 NOTE ON SOURCES FROM 6C- \bar{T} - \bar{C} SUBSEQUENTLY EXCLUDED FROM THIS SAMPLE

6C 0034+375 Our own map at 1.4 GHz from VLA-DnC shows four discrete objects at the following positions: a) 00 33 59.05 +37 52 32.0 (flux density 35.4 mJy), b) 00 34 05.82 +37 33 32.0 (flux density 143.7 mJy), c) 00 34 10.02 37 27 22.0 (flux density 95.8 mJy) and d) 00 35 04.05 36 42 51.1 (flux density 29.6 mJy). Objects a, b, c and d appear to lie on a curved path. It is most likely (from inspection of the 6C-map at 151 MHz) that only b and c are related. Objects a, b and c have counterparts in the 87GB survey and objects a and b have counterparts in the Texas survey. The 6C position falls mid-way between b and c and thus these counterparts were not included by the selection criteria which only searched for counterparts in a $2'$ radius. If b and c form part of one source, then it fails to meet the spectral index selection criterion. Object c alone does not satisfy the 6C flux criteria and object b alone does not satisfy the spectral index criterion. 6C 0034+375 is thus excluded from the 6C* sample.

6C 0059+506 There is an object in the 87GB catalogue which is further than $2'$ away from the 6C po-

sition, at 00 59 03.4 +50 38 51, with flux 94 ± 11 mJy. From our own VLA maps we see that this may be identified with the the north hotspot. The spectral index of this north hotspot derived using the 87GB flux density and the 6C flux density is too flat for this source to remain in this sample.

6C 0104+318 This radio source is probably a mixture of background source lying in the tail of 3C31 and 3C31 tail emission itself (Laycock 1990). It is thus excluded from the 6C* sample as it is unlikely that it satisfies the 6C criterion for flux density.

6 CONCLUDING REMARKS

The search for $z > 4$ radio galaxies requires optical follow-up of relatively faint ($S_{151} \sim 1$ Jy) surveys covering at least ~ 0.1 sr and hence criteria more selective than a simple radio flux density limit. Using data from low resolution (i.e., a few arcminutes) surveys we have applied spectral index and angular size criteria to filter the 279 6C sources with $0.96 < S_{151} < 2.0$ in a 0.133 sr patch of sky to a well defined sample of 34. VLA data show that 27 of these objects (79%) have true angular sizes less than the target upper value of 15 arcsec. A combination of survey and VLA spectral data show that 30 (88%) objects have spectral indices at (observed) 1 GHz greater than a (nominal) target of 0.981. When spectra were fitted to data available from the surveys, only one of the 34 objects showed evidence for a curved spectrum. The inclusion of flux densities from our VLA observations revealed that 10 of the 34 objects show significant concave spectral curvature.

ACKNOWLEDGMENTS

It is a pleasure to thank the staff of the VLA, especially Meri Stanley and Rick Perley for their assistance; we are particularly grateful to Barry Clark whose allocation of discretionary VLA time allowed this project to be started. The VLA is a facility of the National Radio Astronomy Observatory operated by Associated Universities, Inc., under co-operative agreement with the National Science Foundation. The Texas catalogue was obtained using the Einstein On-Line Service, Smithsonian Astrophysical Observatory. This research has made use of the NASA/IPAC Extragalactic Database, which is operated by the Jet Propulsion Laboratory, Caltech, under contract with the National Aeronautics and Space Administration. We thank David Spence help with the figures and Gavin Dalton and Clive Davenhall for their expert computing assistance. We are particularly grateful to Sally Hales who provided a preliminary version of the 6C catalogue prior to publication. Warm thanks are due to Devinder Sivia for providing some of the software used in the fitting of radio spectral indices and for enlightening discussions.

REFERENCES

- Baldwin J.E., Boysen R.C., Hales S.E.G., Jennings J.E., Waggett P.C., Warner P.J., Wilson D.M.A., 1985, MNRAS, 217, 717
- Chambers K.C., Miley G.K., van Breugel W.J.M., 1990, ApJ, 363, 21
- Chambers K.C., Miley G.K., van Breugel W.J.M., Huang J.-S., 1997, ApJS, in press.
- Condon J., Broderick J., 1986. AJ, 91, 1051
- Colla G., Fanti C., Fanti R., Ficarra A., Formigini L., Gandolfi E., Grueff G., Lari C., Padrielli L., Roffi G., Tomasi P., Vigotti M., 1970, AASS, 1, 281
- Colla G., Fanti C., Fanti R., Ficarra A., Formigini L., Gandolfi E., Gioia I., Lari C., Marano B., Padrielli L., Tomasi P., 1973, AASS, 11, 291
- de Ruiter H.R., Parma P., Fanti C., Fanti R., 1986, AASS, 65, 111
- Douglas J.N., Bash F.N., Bozyan F.A., Torrence G.W., Wolfe C., 1996, AJ, 111, 1945
- Dunlop J.S., Peacock J.A., 1990, MNRAS, 247, 19
- Eales S.A., Alexander, P., Duncan, W.D., 1989, MNRAS, 240, 817
- Eales S.A., Rawlings S., 1996, ApJ, 460, 68
- Eales S.A., Rawlings S., Law-Green D., Cotter G., Lacy M., 1997, MNRAS, in press.
- Ficarra A., Grueff G., Tomassetti G., 1985, AASS, 59, 255
- Gregory P.C., Condon J.J., 1991, ApJSS, 75, 1011
- Gull S.F., 1988, in Maximum Entropy and Bayesian methods in science and engineering, Vol 1 (ed. G.J. Erickson & C.R. Smith). Kluwer, Dordrecht.
- Hales S.E.G., Baldwin J.E., Warner P.J., 1988, MNRAS, 234, 919
- Hales S.E.G., Baldwin J.E., Warner P.J., 1993, MNRAS, 263, 25
- Laing R.A., Peacock, J.A., 1980, MNRAS, 190, 903
- Laing R.A., Riley J.M., Longair M.S., 1983, MNRAS, 204, 151
- Lacy M. et al., 1994, MNRAS, 271, 504
- Laycock S., Ph.D. Thesis, University of Cambridge, 1990
- McCarthy P.J., 1993, ARAA, 31, 639
- McGilchrist M.M., Baldwin J.E., Riley J.M., Titterton D.J., Waldram E.M., Warner P.J., 1990, MNRAS, 246, 110
- Neerer M.J., Eales S.A., Law-Green J.D., Leahy J.P., Rawlings S., 1995, 451, 76
- Rawlings S., Lacy M., Blundell K.M., Eales S.A., Bunker A.J., Garrington S.T., 1996, Nature, 383, 502
- Rhee G. Marvel K., Wilson T., Roland J., Bremer M., Jackson N., Webb J., 1996, ApJSS, 107, 175
- Röttgering H.J.A., Lacy M., Miley G.K., Chambers K.C., Saunders R., 1994, A&AS, 108, 79
- Sivia, D.S., 1996, Data Analysis: a Bayesian Tutorial, OUP.
- Vigotti M., Grueff G., Perley R., Clark B.G., Bridle A.H., 1989, AJ, 98, 419
- White R.L., Becker R.H., 1992, ApJS, 79, 331

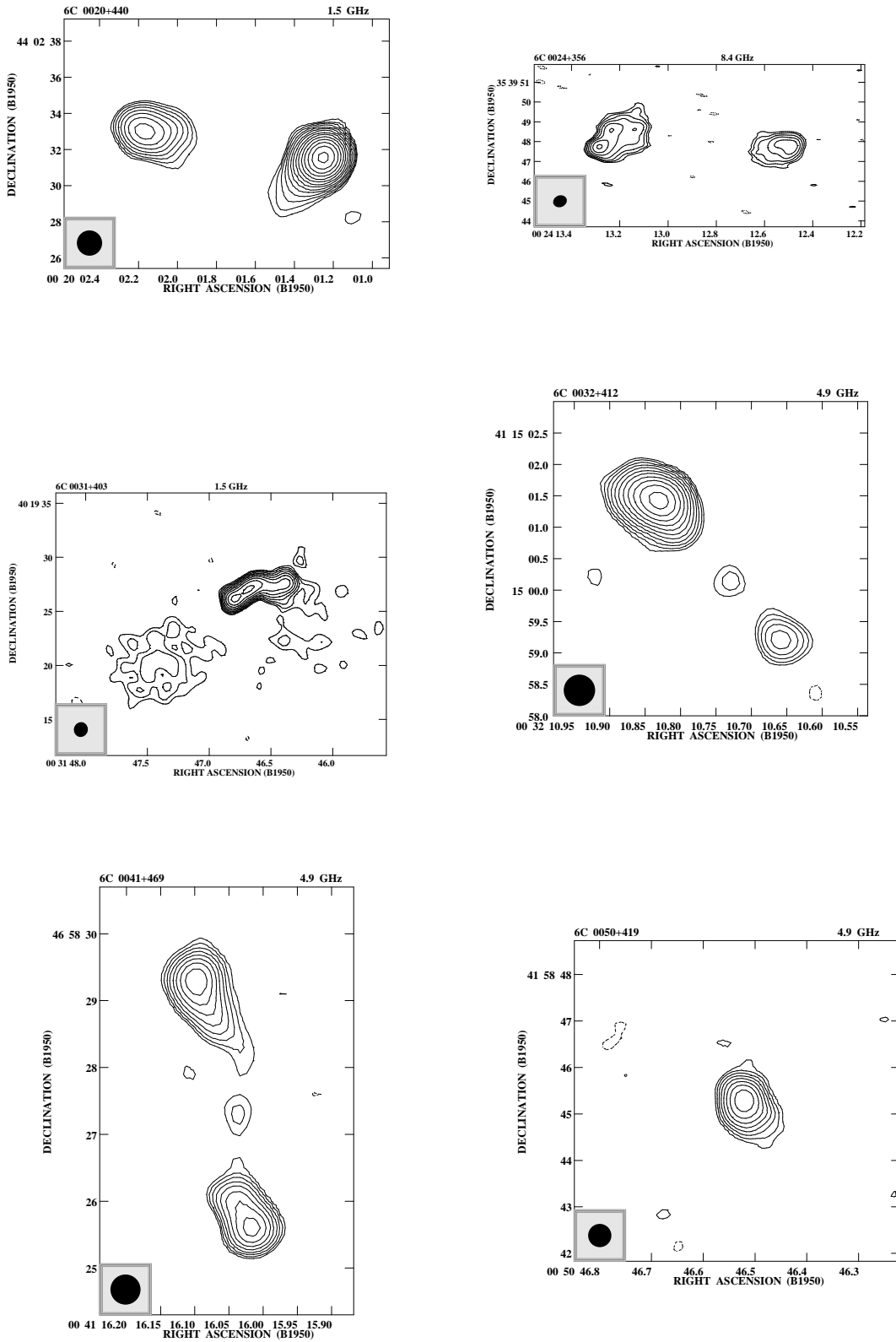


Figure 6. Contour maps of the radio sources.

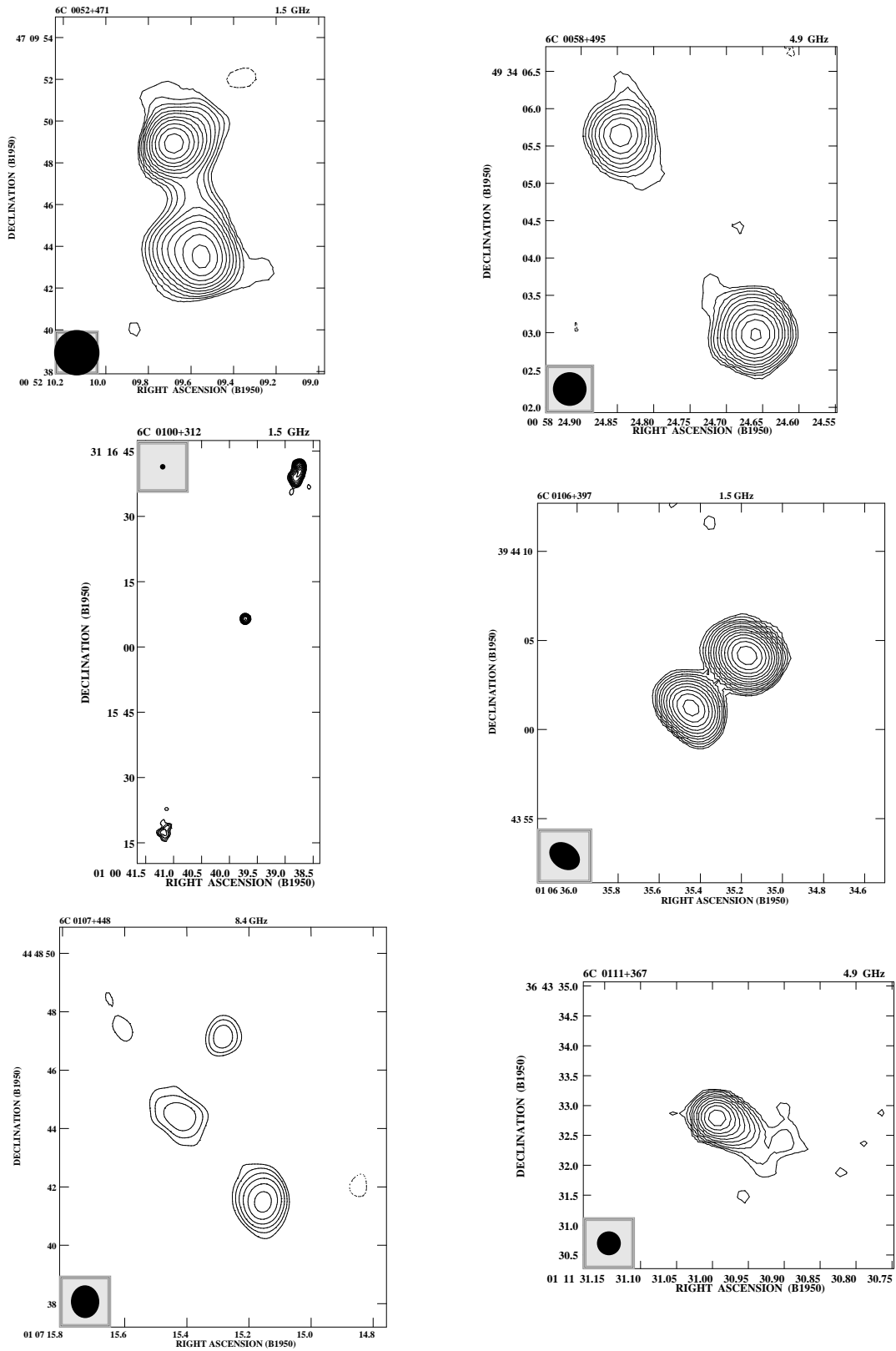


Figure 7. Contour maps of the radio sources.

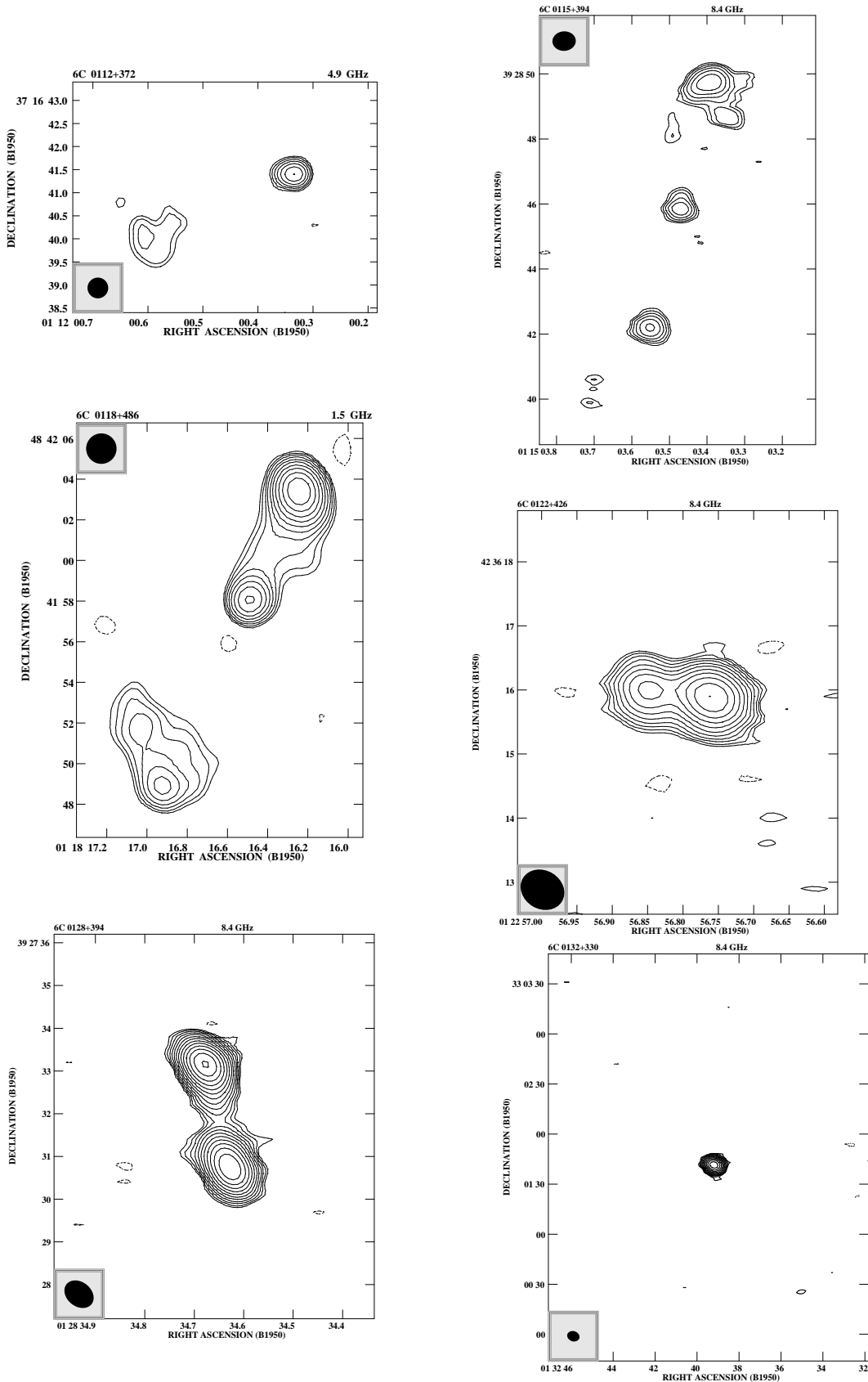


Figure 8. Contour maps of the radio sources.

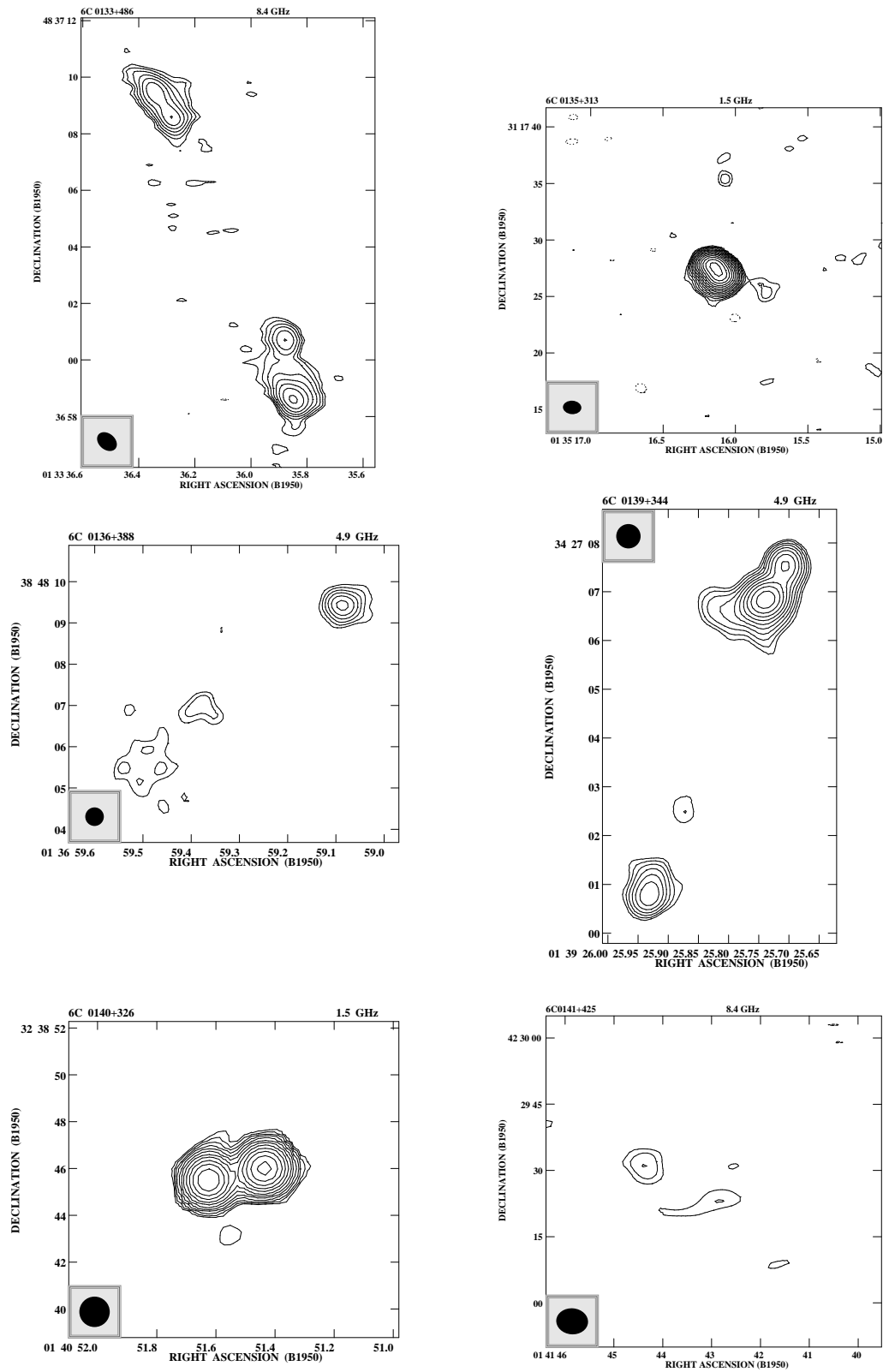


Figure 9. Contour maps of the radio sources.

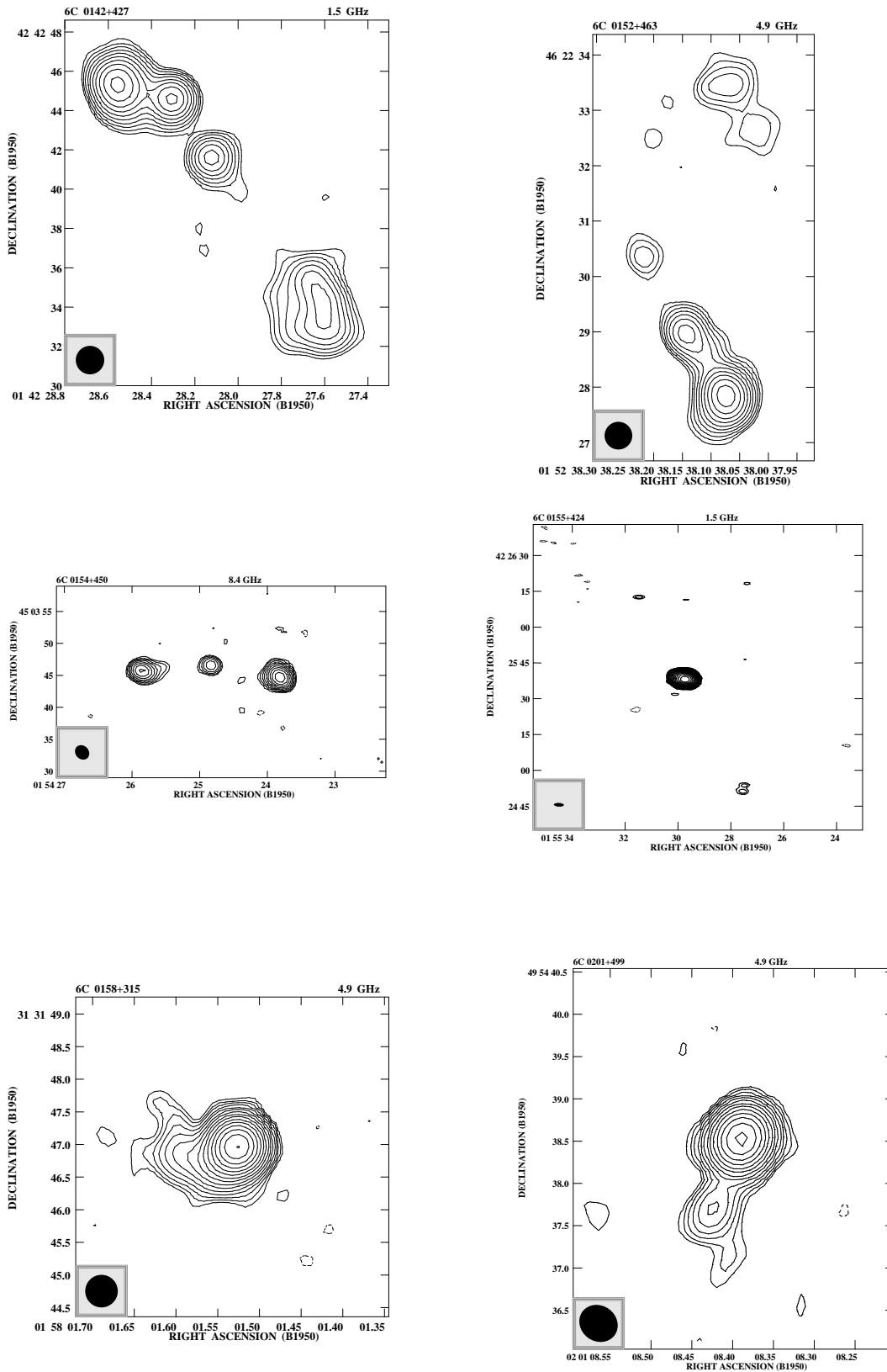


Figure 10. Contour maps of the radio sources.

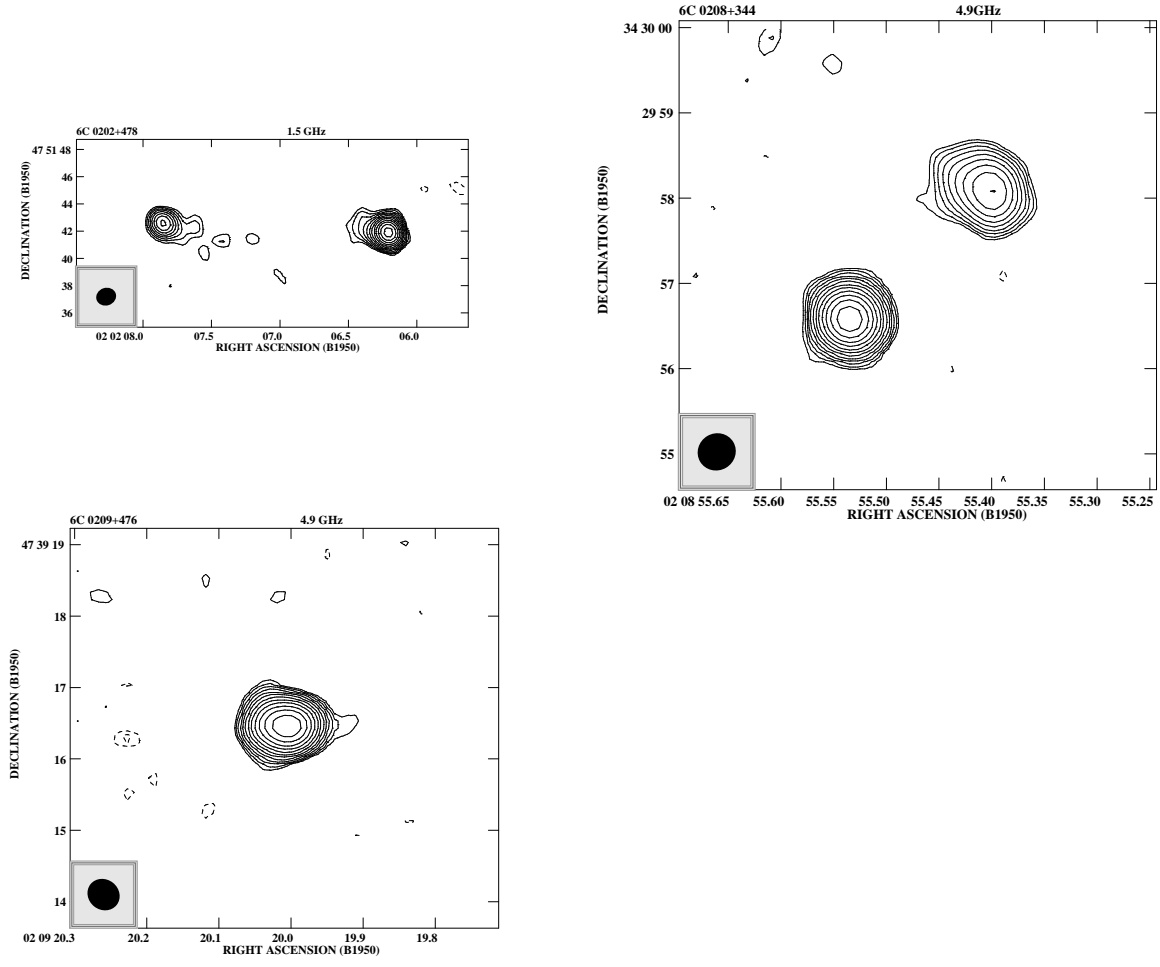


Figure 11. Contour maps of the radio sources.